A unitary coupled-channel approach to J/ψ radiative decay to pseudoscalar pairs*

Yang-hong Lu (卢泱宏)[1,2†] Jia-jun Wu (吴佳俊)[2,3] Bei-jiang Liu (刘北江)[1,2] Xiao-yan Shen (沈肖雁)[1,2]

[1]Institute of High Energy Physics, Chinese Academy of Sciences, Beijing 100049, China
[2]University of Chinese Academy of Sciences, Chinese Academy of Sciences, Beijing 100049, China
[3]Southern Center for Nuclear-Science Theory (SCNT), Institute of Modern Physics, Chinese Academy of Sciences, Huizhou 516000, China

Abstract: We present a comprehensive theoretical approach for describing the amplitude of the processes $J/\psi \to \gamma ab$, where a and b are pseudoscalar mesons. Our approach systematically incorporates final-state rescattering between the pseudoscalar pair ab, contributions from intermediate resonances, and coupled-channel effects via rescattering of a with an intermediate state $\bar{X}$ (which subsequently decays to γb). This formalism ensures unitarity in the two-body rescattering amplitude and dynamically dressed couplings between resonances and the pseudoscalar pair. Using a toy model, we perform numerical calculations and demonstrate that coupled-channel effects significantly influence the lineshape of the invariant mass spectrum of the final states. These findings highlight the necessity of including coupled-channel dynamics in interpretations of J/ψ radiative decays.

Keywords: coupled channel, J/ψ decay, amplitudes analysis, glueball

DOI: 10.1088/1674-1137/ade4a2 **CSTR:** 32044.14.ChinesePhysicsC.49093107

I. INTRODUCTION

Quantum Chromodynamics (QCD), which constitutes the fundamental theory of strong interactions [1], presents one of the most profound challenges in modern physics: the mechanism by which quarks and gluons form hadrons. While perturbative methods successfully describe high-energy regimes, the low-energy domain remains intractable due to nonperturbative phenomena such as color confinement. Recent experimental discoveries of new hadrons [2] have further challenged the conventional quark model, where mesons are understood as quark-antiquark pairs and baryons as three-quark systems. These observations provide critical insights into exotic resonance dynamics and nonperturbative QCD, yet our understanding remains limited by sparse statistical data and incomplete amplitude parameterizations [3]. Many candidates are observed exclusively in single production or decay channels, necessitating rigorous constraints on reaction amplitudes to reduce systematic uncertainties.

Traditional Breit-Wigner (BW) parameterizations suffice for narrow, isolated resonances but fail for overlapping states or those near thresholds. In such cases, preserving fundamental amplitude properties − unitarity (from probability conservation) and analyticity (from causality) − requires more sophisticated coupled-channel frameworks [4]. The K-matrix formalism [5], for instance, enforces unitarity through real matrix elements but suffers from limitations: its fixed matrix structure struggles with new channels, and parameter uncertainties degrade accuracy for high-statistics data. Crucially, it neglects the energy-dependence of the real part of self-energy corrections, leading to inconsistencies in lineshape descriptions and pole extractions [6−8].

A key objective in QCD is the search for glueballs − exotic states dominated by gluonic interactions − which directly probe non-Abelian gauge dynamics. Radiative J/ψ decays to pseudoscalar meson pairs offer a unique window into glueball production, as demonstrated by extensive BESIII studies [9, 10]. These gluon-rich processes are ideal for identifying scalar and tensor glueball candidates [11], though challenges persist due to broad, overlapping resonances and flavor-blind gluonic decays that populate multiple channels [12]. Conventional BW methods are inadequate for resolving these complexities.

In this study, we develop a unitary coupled-channel amplitude for $J/\psi \to \gamma ab$ (where a and b are pseudoscalars), incorporating two-pseudoscalar rescattering via coupled-channel Lippmann-Schwinger (LS) equations [13−16], intermediate meson-photon couplings ($a\bar{X} \to \gamma b$), and energy-dependent self-energies absent in K-matrix approaches. Our framework avoids the pitfalls of the

Received 21 April 2025; Accepted 28 May 2025; Published online 29 May 2025

* Supported partly by the National Natural Science Foundation of China (11935016, 12175239, 12221005, 12235017, 12361141819) and the Chinese Academy of Sciences (YSBR101) (J.J.W and B.J.L)

† E-mail: yhlu@ihep.ac.cn

BW and K-matrix methods by embedding unitary two-body amplitudes directly into the decay process, enabling unbiased resonance property extraction from experimental data. We validate the model's efficacy using toy calculations and demonstrate its application to $J/\psi \to \gamma K_S K_S$.

The remainder of this paper is structured as follows. In the following section, we outline the model construction and formalism. Section III presents the calculation of the $J/\psi \to \gamma K_S K_S$ process as an example of using this formalism. Concluding remarks and a discussion are given in Section IV.

II. FORMALISM

A. Mechanisms of J/ψ radiative decay into two pseudoscalar mesons

We analyze the process $J/\psi \to \gamma ab$, where a and b denote pseudoscalar mesons, incorporating two coupled-channel effects:

1. Rescattering $ab \to ab$: Dominated by intermediate resonances (XY) originating from bare states.

2. Rescattering $\bar{X}a \to \bar{X}'b$: Assumes constant decay widths for $\bar{X}$ (which couples to γa) and neglects $\bar{X}$'s coupled channels.

These approximations are justified because

- Electromagnetic interactions (*e.g.*, photon rescattering) are negligible compared to strong interactions.

- Including $\bar{X}$'s strong decays would require a three-body formalism at least, breaking two-body unitarity − a reasonable trade-off for this work.

The decay processes $J/\psi \to \gamma ab$ can be classified into the four categories illustrated in Fig. 1. In Fig. 1(a), the process corresponds to a direct three-body decay governed by the vertex of $J/\psi\gamma ab$. The contribution of rescattering $a'b' \to ab$ is included in Fig. 1(b). It is worth mentioning that the first vertex shares that in Fig. 1 (a), and the rescattering contribution is described by the full T-matrix of $a'b' \to ab$, which is discussed in detail in the next section. InFig. 1(c), the process corresponds to the bare state X. J/ψ first radiatively decays to the bare state X, and then, X couples to the final ab state. Here, we need a new vertex of $J/\psi\gamma X$, full propagator matrix of bare states X, denoted as A_{XY}, and dressed vertex of Xab. Importantly, the propagator matrix and dressed vertex of Xab are both determined by the T-matrix of the rescattering $a'b' \to ab$. Finally, in Fig. 1(d), we show the contribution of the rescattering of $\bar{X}a$, which is completely independent of the previous three mechanisms. Conventional isobar models (*e.g.*, BW) only include the category shown in Fig. 1(c), violating unitarity for overlapping resonances.

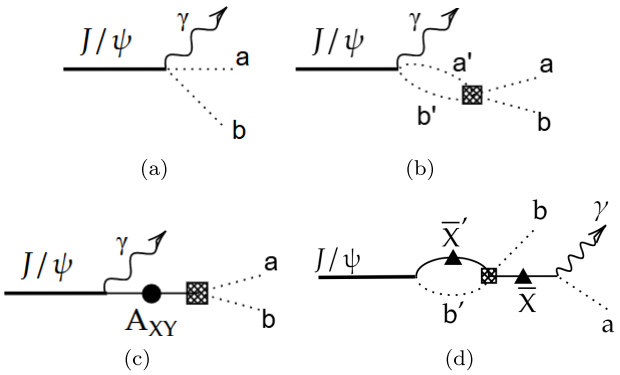

Fig. 1. Diagrams of the four categories of reactions. In this paper, pseudoscalar mesons are represented by dashed lines and bare states by solid lines. Grid-patterned boxes denote coupling vertices associated with specific initial and final states, while solid black circles depict propagators modified through self-energy corrections. Solid black triangles symbolize propagators of bare states with parameter-adjusted properties.

B. Coupled-channel T-matrix

The S-matrix connects the initial and final states, which encodes the probabilities of transitions between them. Because the S-matrix satisfies unitarity for the conservation of probability, *i.e.*, $S^{\dagger}S = 1$, it is well defined and can be expressed through phase shifts and inelasticities, which can be extracted from the experimental observables. Furthermore, the T-matrix calculated from the interaction vertices based on the theoretical models can also be used to derive the S-matrix through the standard scattering theory. However, under different notations, the connection between them may differ. In this paper, we use the following definition for the $2 \to 2$ process [17]:

$$S_{fi} = \delta_{fi} - 2\pi \mathrm{i} \sqrt{\rho_f(E)} T_{fi}(k_{on}, k_{on}; E) \sqrt{\rho_i(E)}, \quad (1)$$

where f and i are for the final and initial states, respectively. $\rho_i(E)$is the state density of the channel i for two body systems:

$$\rho_i(E) = \frac{E_{i1}(k_i)E_{i2}(k_i)}{E} k_i^2, \quad (2)$$

where k_i is defined as the on-shell momentum for channel i, *i.e.*, $E = \sqrt{k_i^2 + m_{i1}^2} + \sqrt{k_i^2 + m_{i2}^2}$, and E is the total energy in their CM frame. Then, the differential cross section between two channels can be expressed as follows:

$$\frac{\mathrm{d}\sigma_{fi}}{\mathrm{d}\Omega} = 4\frac{(2\pi)^4\rho_f(E)\rho_i(E)}{k_i^2}\bar{\sum}|T_{fi}|^2, \tag{3}$$

where $\bar{\sum}$ is for the average of the spin states of initial state i and summation of the spin states of finial state f. In addition, for the differential decay width, it is expressed as

$$\frac{\mathrm{d}\Gamma_{i\to f}}{\mathrm{d}\Omega} = \frac{2\pi\rho_f(E)}{M_i}\bar{\sum}|T_{fi}|^2. \tag{4}$$

Typically, the T-matrix defined here has a factor different from usual covariant amplitude $\mathcal{M}$ defined based on Particle Group data [1] as follows:

$$T_{fi} = \frac{1}{(2\pi)^3}\sqrt{\frac{1}{2E_{i1}2E_{i2}2E_{f1}2E_{f2}}}\mathcal{M}_{fi} \tag{5}$$

for $2\to 2$ and

$$T_{fi} = \frac{1}{(2\pi)^{3/2}}\sqrt{\frac{1}{2M_i2E_{f1}2E_{f2}}}\mathcal{M}_{fi} \tag{6}$$

for $1\to 2$. It is related to the definition of the LS equation to solve the T-matrix. Here, the symbol fi refers to the final and initial states, while T_{fi} represents the T-matrix elements.

The LS equation, defined in the center-mass system (CMS) of the final two-body system, is formulated as follows for the fixed partial wave denoted by angular momentum L:

$$\tilde{T}^L_{\alpha\beta}(k,k';E) = \tilde{V}^L_{\alpha\beta}(k,k';E) + \sum_\gamma\int \mathrm{d}q\, q^2\frac{\tilde{V}^L_{\alpha\gamma}(k,q;E)\tilde{T}^L_{\gamma\beta}(q,k';E)}{E-\omega_\gamma(q)+i\epsilon}, \tag{7}$$

where the potential $\tilde{V}^L$ between two coupled channels includes contributions from bare states with spins $J=L$ and the direct vertices. Here, α and β refer to the final and initial states because the two sides of re-scattering are one of the considered channels. $T^L_{\alpha\beta}$ is the partial wave amplitude for $\alpha\to\beta$ with angular monument L. The on-shell energy ω_γ of the given channel is defined as $\omega_\gamma(q) = \sqrt{m_1^2+q^2}+\sqrt{m_2^2+q^2}$. The corresponding diagrams for the processes $2\to 2$ and $1\to 2$ are shown in Figs. 2(a) and (b), respectively.

The potential $\tilde{V}^L_{\alpha\beta}(k,k',E)$ comprises two terms,

$$\tilde{V}^L_{\alpha\beta}(k,k',E) = V^L_{\alpha\beta}(k,k') + \sum_X\frac{G^L_{X\alpha}(k)G^L_{X\beta}(k')}{E-m_X+\mathrm{i}\epsilon}, \tag{8}$$

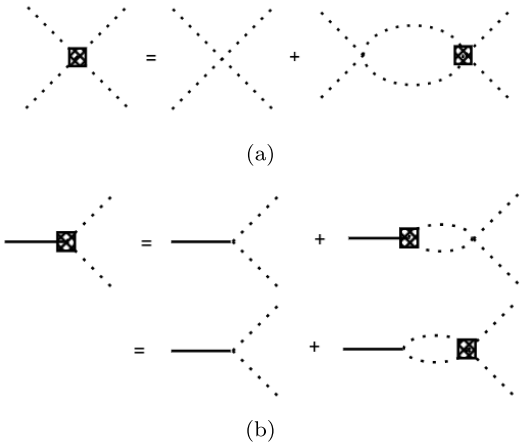

Fig. 2. LS equation for coupled vertexes: (a) $2\to 2$ and (b) $1\to 2$.

where $V^L_{\alpha\beta}(k,k')$ is the bare-state-independent potential between two channels (energy-independent of E), while coupling function $G_{X\alpha}$ describes the coupling between bare state X with bare mass m_X and channel α. Note that the spins of these X should be equal to L. The potential $V^L_{\alpha\beta}(k,k')$ typically includes t- and u-channel exchanges as well as the contact term. However, for interpolating the scattering data in the finite energy region, separable potential form is a reasonable way to parameterize this potential. Furthermore, such a separable potential promises an exact analytical solution to the LS equation; thus, we choose the following form of $v_{\alpha\beta}(k,k')$:

$$V^L_{\alpha\beta}(k,k') = v^L_{\alpha\beta}f^L_\alpha(k)f^L_\beta(k'), \tag{9}$$

$$f^L_\alpha(k) = \frac{\left(1+\frac{k^2}{\Lambda^2}\right)^{-2-L/2}\cdot(k/m_0)^L}{\sqrt{E_{\alpha_1}(k)E_{\alpha_2}(k)}}, \tag{10}$$

where Λ is the QCD energy cut around 1 GeV, m_0 is the representative meson mass and usually takes the value m_{π_0}, and $v^L_{\alpha\beta}$ is a real number that indicates the coupling constant between channel α and β in the partial wave L. The vertex of the bare state X and channel α, $G^L_{X\alpha}(k)$, can be expressed as

$$G^L_{X\alpha}(k) = g^L_{X\alpha}\frac{m_0}{\sqrt{m_X}}f^L_\alpha(k), \tag{11}$$

where $g^L_{\alpha X}$ is a real dimensionless coupling strength constant.

Based on Eq. (8), the solution of the LS equation in Eq. (7) is the T-matrix, $\tilde{T}^L$, which can be decomposed into two components as follows:

$$\tilde{T}^L = t^L + T^L. \tag{12}$$

These two parts t^L and T^L indicate the contribution from the channels without and with the bare states with the same orbital angular moments L and same matrix elements $\alpha\beta$, respectively.

t^L is defined as

$$t^L_{\alpha\beta}(k,k';E) = V^L_{\alpha\beta}(k,k') + \sum_\gamma \int \mathrm{d}q\, q^2 \frac{V^L_{\alpha\gamma}(k,q) t^L_{\gamma\beta}(q,k';E)}{E-\omega_\gamma(q)+\mathrm{i}\epsilon}. \tag{13}$$

Adopting the separable potential $V^L_{\alpha\beta}$ as shown in Eq. (9), the solution of $t^L_{\alpha\beta}$ inherits a similar separable form as follows:

$$t^L_{\alpha\beta}(k,k',E) = f^L_\alpha(k)\tilde{t}^L_{\alpha\beta}(E) f^L_\beta(k'), \tag{14}$$

where

$$\tilde{t}^L_{\alpha\beta}(E) = \sum_\gamma \left(I - v^L M(E)\right)^{-1}_{\alpha\gamma} v^L_{\gamma\beta}. \tag{15}$$

Here, I is a unit matrix, the elements of the matrix v^L are $v_{\alpha\beta}$, and the diagonal matrix $M(E)$ is defined as follows:

$$M_{\alpha\alpha}(E) = \int \frac{q^2 \mathrm{d}q |f_\alpha(q)|^2}{E - w_\alpha(q) + \mathrm{i}\epsilon}. \tag{16}$$

The second term at the right side of Eq. (12), T^L, is derived as

$$T^L_{\alpha\beta}(k,k',E) = \sum_{XY} \mathcal{G}^L_{\alpha X} A_{XY} \mathcal{G}^L_{Y\beta}, \tag{17}$$

where $\mathcal{G}^L_{\alpha X}$ and $\mathcal{G}^L_{Y\beta}$ are the dressed coupling functions of $X \to \alpha$ and $\beta \to Y$, respectively, and A_{XY} is the dressed propagator between the bare state X and Y. The two dressed coupling functions can be derived as

$$\mathcal{G}^L_{X\alpha}(k;E) = G^L_{X\alpha}(k) + \sum_\gamma g_{X\gamma}(E)\tilde{t}^L_{\gamma\alpha}(E) f_\alpha(k), \tag{18}$$

$$\mathcal{G}^L_{\alpha X}(k;E) = G^L_{X\alpha}(k) + \sum_\gamma f_\alpha(k)\tilde{t}^L_{\alpha\gamma}(E) g_{X\gamma}(E), \tag{19}$$

with

$$g_{X\gamma}(E) = \int \mathrm{d}q\, q^2 \frac{G_{X\gamma}(q) f_\gamma(q)}{E - \omega_\gamma(q) + \mathrm{i}\epsilon}. \tag{20}$$

In contrast, the T-matrix of $1 \to 2$ is indeed $\mathcal{G}^L_{X\alpha}(k;E)$. The dressed propagator of the bare states is a matrix, and elements of its inverse matrix can be expressed as follows:

$$(A^{-1})_{XY}(E) = \delta_{XY}(E - m_X) - \Sigma^0_{XY}(E) - \Sigma^I_{XY}(E), \tag{21}$$

where

$$\Sigma^0_{XY}(E) = \sum_\gamma \int \mathrm{d}q q^2 \frac{G_{X\gamma}(q) G_{Y\gamma}(q)}{E - \omega_\gamma(k) + \mathrm{i}\epsilon}, \tag{22}$$

is the self energy of

$$\Sigma^{\mathrm{I}}_{XY}(E) = \sum_{\alpha,\beta} g_{X\alpha}(E)\tilde{t}^L_{\alpha\beta}(E) g_{Y\beta}(E). \tag{23}$$

The corresponding diagram is shown in Fig. 3.

Finally, we consider the rescattering between $\bar{X}$ and a. As discussed in the previous subsection, $\bar{X}$ can decay, implying that this scattering process inherently involves the effect of three-body unitary, which is beyond the current model. As shown in Fig. 4, the two right diagrams in the first line show the three-body contribution, and the intermediate state could be the three states described by dashed lines. Then, we make the assumption that we use a contact term to describe the interaction between $\bar{X}$ and a, illustrated by the first diagram in the second line. For the triangle loop, we directly absorb it into the width of $\bar{X}$, which is indicated by the solid triangle in the right diagram in the second line of Fig. 4. Then, the energy term of $\bar{X}$ is replaced as a complex energy $E - \mathrm{i}\Gamma/2$, where Γ denotes the width. Consequently, analogous to the solution of the LS equation mentioned earlier without the bare state contribution, as shown in Eq. (12), with the same separable potential form, we can obtain

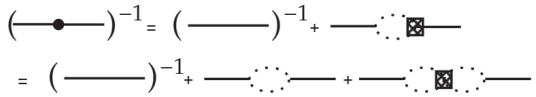

Fig. 3. Self-energy corrections for propagator.

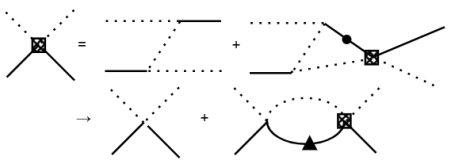

Fig. 4. Diagrams of the scattering between $\bar{X}$ and a. The Z diagram and triangle loop are proximate to the contact term and two particles loop with a fitted parameter of width $\bar{X}$.

$$\bar{t} = (1 - \bar{v}\bar{M})^{-1}\bar{v}, \tag{24}$$

$$\bar{M}_{(aX)} = \int \mathrm{d}q\, q^2 \frac{|f_{(aX)}(q)|^2}{E - \omega_{(aX)}(q) + \mathrm{i}\Gamma/2}, \tag{25}$$

where $\bar{v}$ is the coupling constant matrix.

C. Partial wave amplitudes

In the preceding subsection, we obtained the propagators and coupling vertices involved in the four mechanisms of Fig. 1. The dynamical component of the scattering amplitude is an explicit product of these factors, so it remains only to introduce the angular distribution components to obtain the complete partial wave amplitude. Here, we incorporate the partial wave amplitudes to account for the angular distributions. For the background terms and two processes involving ab scattering, we must consider two angular momentum degrees of freedom, while for the $\bar{X}a$ process, three degrees of freedom must be taken into account. Consequently, the four reaction amplitudes including the orbital angular momentum can be expressed for an output channel (α) and photon (γ) as

$$\begin{aligned}\mathcal{M}^{(a)}_{J/\psi\to\,\gamma\alpha} = & \sum_{L_1,L_2,L_1^z,L_2^z,S,S^z} \langle 1S_\gamma^z, L_2L_2^z|SS^z\rangle \\ & \times \langle SS^z, L_1L_1^z|1S^z_{J/\psi}\rangle \\ & \times u^{L_1L_2S}_{J/\psi\to\,\gamma\alpha} Y_{L_1L_1^z}(-\hat{q}_\gamma) f^{L_1}_{(J/\psi,\gamma)}(q_\gamma) \\ & \times Y_{L_2L_2^z}(\hat{q}_\alpha) f^{L2}_{\alpha}(q_\alpha),\end{aligned} \tag{26a}$$

$$\begin{aligned}\mathcal{M}^{(b)}_{J/\psi\to\,\gamma\alpha} = & \sum_{L_1,L_2,L_1^z,L_2^z,S,S^z} Y_{L_1L_1^z}(-\hat{q}_\gamma) f^{L_1}_{(J/\psi,\gamma)}(q_\gamma) \\ & \times \langle 1S_\gamma^z, L_2L_2^z|SS^z\rangle\langle SS^z, L_1L_1^z|1S^z_{J/\psi}\rangle \\ & \times \sum_\beta u^{L_1L_2S}_{J/\psi\to\,\gamma\beta} M^{L_2}_{\beta\beta}(E)\tilde{t}^{L_2}_{\beta\alpha}(E) f^{L_2}_{\alpha}(q_\alpha) Y_{L_2L_2^z}(\hat{q}_\alpha)\end{aligned} \tag{26b}$$

$$\begin{aligned}\mathcal{M}^{(c)}_{J/\psi\to\,\gamma\alpha} = & \sum_{L_1,L_2,L_1^z,L_2^z,S,S^z} Y_{L_1L_1^z}(-\hat{q}_\gamma) f^{L_1}_{(J/\psi,\gamma)}(q_\gamma) \\ & \times \langle 1S_\gamma^z, L_2L_2^z|SS^z\rangle\langle SS^z, L_1L_1^z|1S^z_{J/\psi}\rangle \\ & \times \sum_{XY} u^{L_1L_2S}_{J/\psi\to\,\gamma X} A_{XY}(E)\mathcal{G}^{L_2}_{Y\alpha}(q_\alpha, E) Y_{L_2L_2^z}(\hat{q}_\alpha)\end{aligned} \tag{26c}$$

$$\begin{aligned}\mathcal{M}^{(d)}_{J/\psi\to\,\gamma\alpha} = & \sum_{L_1,L_1^z}\sum_{\bar{Y}c,S^z_{\bar{X}}} Y^*_{L_1L_1^z}(\hat{q}_c)\langle S_{\bar{Y}}S^z_{\bar{Y}}, L_1L_1^z|1S^z_{J/\psi}\rangle \\ & \times u^{L_1}_{J/\psi\to\,\bar{Y}c}\bar{M}_{\bar{Y}c}(m_{J/\psi}) \\ & \times \sum_{L_2,L_2^z}\sum_{\bar{X},S^z_{\bar{X}}}\langle S_{\bar{X}}S^z_{\bar{X}}, L_2L_2^z|1S^z_{J/\psi}\rangle Y_{L_2L_2^z}(\hat{q}_b) \\ & \times \bar{t}_{\bar{Y}c\bar{X}b}(m_{J/\psi}) f^{L_1}_{\bar{X}b}(q_b) \\ & \times \sum_{L_3L_3^z}\langle 1S^z_\gamma, L_3L_3^z|S_{\bar{X}}S^z_{\bar{X}}\rangle Y_{L_3L_3^z}(-\hat{q}_\gamma) \\ & \times \frac{f^{L_3}_{\bar{X}\to\gamma a}(q_a)}{E(q_a) - m_{\bar{X}} + \mathrm{i}\Gamma/2},\end{aligned} \tag{26d}$$

Here, the three related momenta are all the back-to-back moments in their CMS frame, where dynamic factors like f^L, t^L, M^L, A^L, and $\mathcal{G}^L$ are defined in the last subsection. The spherical harmonics terms Y_{LL^z} with Clebsch-Gordan coefficients are involved to describe the angular moment contributions for the partial wave amplitudes.

$u^{L_1L_2S}_{J/\psi\to\gamma\alpha(X)}$ refers to the coupling strength constants of their subscript processes, where L_1, L_2, and S are the angular momentum between γ and $\alpha(X)$, total spin of α channel (or the spin of X), and total spin of $\gamma\alpha(X)$, respectively. Here, we do not give a detailed expansion because the relative partial-wave amplitudes are given explicitly in Ref. [18]. To clarify the notation, we give an example for X with $J^P = 0^-$. In this case, only one partial wave survives, with $L_1 = 1$, $L_2 = 0$, and $S = 1$:

$$u^{L_1L_2S}_{J/\psi\to\gamma\alpha(X)} = \epsilon_{\mu\nu\alpha\beta}\epsilon^\mu_{J/\psi}\epsilon^{*\nu}_\gamma P^\beta_{(J/\psi)}\tilde{t}^{(1)\alpha}, \tag{27}$$

where $\tilde{t}^{(1)\alpha}$ is the p-wave vertex of the γ and X, as defined in Ref. [18].

D. Comparison with other methods

Recognizing the importance and relevance of the comparison between our Lippmann-Schwinger (LS) formalism and the K-matrix, as well as other approaches, we provide a detailed discussion in this subsection.

First, as we pointed out in the introduction, because the K-matrix method neglects the energy-dependence of the real part of self-energy, it can be modified by introducing $K = (1 - VG')V$, where G' is the Chew-Mandelstam variable and V is a potential. However, such methods still have significant limitations. The potentials V or K remain independent of the loop integration, which implies that an on-shell approximation is applied to both V and K. While this framework may provide adequate data fitting, its predictive capabilities can be questionable.

In our method, we definitely include the off-shell contribution of potential in the loop integration. As shown in Eq. (16), the M matrix replaces the pure two point loop

integration in the K-matrix method combined with Chew-Mandelstam variables or the iρ term in the pure K-matrix method. The M matrix incorporates form factor details from the potential, which indicates that the off-shell contribution is reasonably included. Furthermore, this potential is established through theoretical interpolation, with various parameters tightly constrained by symmetries like chiral Lagrangians or $SU(3)$ symmetry. Accordingly, during data fitting, these parameters benefit from robust theoretical constraint.

Conducting a numerical comparison involves inherent challenges, primarily due to the need for identical potentials when comparing the LS approach with the K-matrix approach, or using both to fit similar datasets to evaluate pole positions. Previous work [19] has explored the prediction of the P_c state, offering detailed comparisons between our LS approach and the Valenca method, a variant of the K-matrix+Chew-Mandelstam approach. Using identical potentials, these calculations yield differing predictions for the mass of the P_c state. Notably, the LS approach predicts a smaller binding energy, more closely aligning with experimental measurements at the LHCb. As such, we do not repeat these calculations here. Later, we will employ a toy model to illustrate the impact of coupled channel contributions.

Finally, we discuss the relativistic corrections. Relativistic corrections encompass two primary components: kinematic alterations and particle-antiparticle generation from vacuum states. Our methodology incorporates the first through a relativistic dispersion relation. However, the second — which is often overlooked at the hadronic level — remains unsolved in the context of the four-dimensional BS equation. The LS approach effectively employs a three-dimensional reduction. This reduction remains justified at the hadronic level; for example, the pion, as the lightest hadron, has a mass of approximately 100 MeV, permitting the neglect of antiparticle contributions during propagation. Nevertheless, if current quark structures constitute the foundation of the theory, these relativistic corrections become more pronounced. Presently, such a non-relativistic approach is prevalently adopted in hadronic physics.

This section provides a comprehensive discourse on the comparative strengths and limitations of the various methodologies, highlighting our advancements and situating them within existing theoretical frameworks.

III. NUMERICAL RESULTS: TOY MODEL ANALYSIS

To demonstrate the significance of the coupled-channel effect, we apply our framework to the decay $J/\psi \to \gamma K_S K_S$. In this toy model, we include two pseudoscalar coupled channels ($K_S K_S$ and $\pi_0\pi_0$, with bare masses set to their PDG values [1]), along with two bare states ($J^{PC} = 0^+$): an f_0 with a bare mass of 1.221 GeV and $f_0^{'}$ at 1.451 GeV. In addition, we include a K_1 state ($J^{PC} = 1^+$) with a mass of 1.403 GeV and width of 0.174 GeV for the γK_S channel. For simplicity, we restrict our analysis to S-wave partial wave amplitudes. The model parameters are listed in Tables 1 and 2.

We first determine the pole positions of the T-matrix in the complex energy plane for the two-pseudoscalar coupled channels by solving $Det[A_{XY}(E)^{-1}] = 0$ on the relevant Riemann sheets. For the ab coupled channels, we identify two pole positions in the second Riemann sheets (denoted as uu), as summarized in Table 3. For the $K_1 K_S$ channel, the width in the K_1 propagator is pre-set, and its pole position is fixed to $M_{\rm poles} = m_{\rm bare} - {\rm i}\Gamma/2$. While the real and imaginary parts of the pole position in a unitary model generally differ from the BW mass and width, they converge for narrow resonances [20]. Our model shows that the two f_0 resonances, generated via the bare-state couplings, exhibit narrow widths, resulting in invariant mass peaks consistent with their pole positions. In contrast, the broader K_1 resonance ($\Gamma \approx 150$ MeV) undergoes significant lineshape modifications due to $K_1 K_S \to K_1 K_S$ rescattering, leading to an observable

Table 1. Parameters for the considered Dual-Channel Decay PP Model. The meaning of each parameter is defined in the description provided in the previous section. All energy units are GeV, and the QCD energy cutoffs Λ are fixed at 1 GeV.

$R\ \{L\}$	$f_0\ \{0\}$	$f_0^{'}\ \{1\}$
m_R	1.221	1.457
$g_{(R,KK)}$	0.810	−0.710
$g_{(R,\pi\pi)}$	−0.740	0.910
$u_{(J/\psi,\gamma R)}$	0.300	0.500
γPP		
$v_{KK,KK}$	0.980	–
$v_{KK,\pi\pi}$	0.870	–
$v_{\pi\pi,\pi\pi}$	0.980	–
$u_{(J/\psi,\gamma KK)}$	0.800	–
$u_{(J/\psi,\gamma\pi\pi)}$	0.800	–

Table 2. Parameters for the considered dual-channel decay XP model. See Table 1 for descriptions.

$R\ \{L\}$	$K_1\ \{0\}$	
m_R	1.403	–
Γ_R	0.174	–
$\bar{u}_{(J/\psi,KR)}$	1.400	–
$\bar{v}_{(KR,KR)}$	1.000	–
$\bar{g}_{(R,\gamma K)}$	1.000	–

Table 3. Pole positions in PP scattering case amplitudes. Their Riemann sheets are specified by $(KK,\pi\pi)$. For the K_1 resonance, we take its pole position from the BW form. The real part is very close to the input mass of K_1, and the imagery part is obtain by $\mathrm{Im}(M_{\rm pole}) = -\Gamma(\mathrm{Res})/2$.

$R\{L\}$	$M_{\rm pole}$/GeV	RS
$f_0\{0\}$	$1.225-0.010\,\mathrm{i}$	(uu)
$f_0^{'}\{0\}$	$1.457-0.007\,\mathrm{i}$	(uu)
$K_1\{0\}$	$1.403-0.087\,\mathrm{i}$	–

shift in the γK_S invariant mass spectrum.

We now present the Daliz plots for the reaction. The distributions of the sum of Fig. 1(a)−(c), pure Fig. 1(d), and full amplitudes are shown in Fig. 5(a)−(c), respectively. Two clear f_0 signals presented as red lines in Fig. 5(a) and one signal for K_1, as shown by the blue broad belt in Fig. 5(b), emerge, corresponding to the intermediate states in our model. Interference between these components significantly distorts the K_1 lineshape, underscoring the necessity of including all mechanisms. An enhancement is observed at high $M_{K_SK_S}$ and low $M_{\gamma K_S}$, arising from interference between the tree-level diagram and dynamical rescattering effects.

To elucidate the contributions of dynamical mechanisms, Fig. 6 decomposes the contributions of individual mechanisms. We find that the mechanism shown in Fig. 1(c) provides the primary contribution to two f_0 resonance peaks, while Fig. 1(a) and (b) remain essentially flat. However, their interference enhances contributions in the high-energy region of $M_{K_SK_S}$ and also strengthens the background under both f_0 resonance peaks. Thus, the analysis demonstrates that the coupled-channel model is crucial for a unified treatment of various background contributions, and the correct description of the background is also extremely important for extracting resonance structures. Regarding the mechanism shown in Fig. 1(d), it does not produce any special structure in the invariant mass spectrum of K_SK_S but generates a subtle bump via interference from other channels in the high-energy region. This explains the observed statistical enhancement in the high $M_{K_SK_S}$ region in the Dalitz plot. Similarly, in the γK invariant mass spectrum, the $\bar{X}b$ rescattering shown in Fig. 1(d) clearly dominates the peak structure, which undergoes a measurable shift due to the interference with contributions of Fig. 1(a)−(c). These results highlight the critical role of coupled-channel effects in resonance analysis: interference can distort lineshapes from simple BW expectations, necessitating a unified framework for accurate mass/width extraction.

IV. SUMMARY AND OUTLOOK

In this study, we developed a unitary coupled-channel framework for a system of two pseudoscalar mesons,

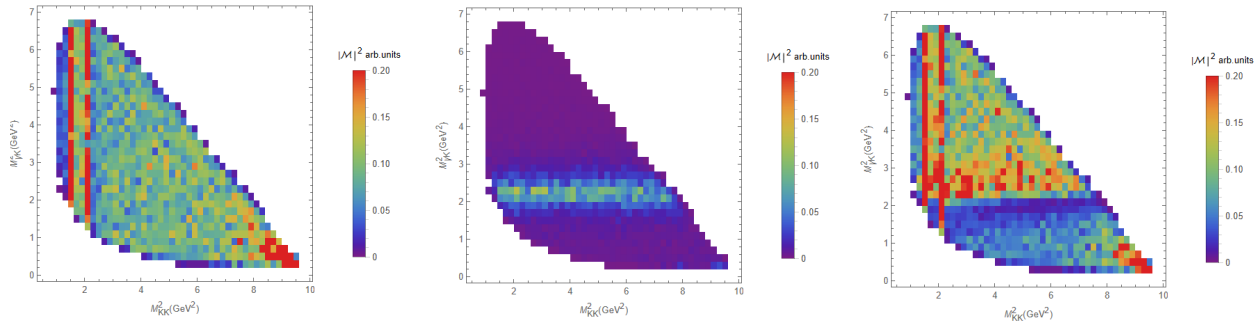

Fig. 5. (color online) Dalitz plot on $M^2(KK)$ and $M^2(\gamma K)$for different squared amplitudes. (a) Tree-level, PP-rescattering, and Bare states; (b) XP-rescattering; and (c) all amplitudes.

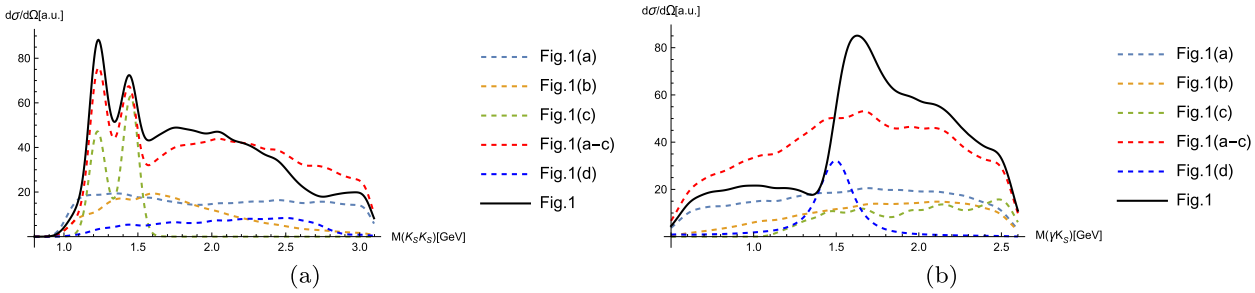

Fig. 6. (color online) One-dimensional projection plot for each amplitude on $M(\gamma K)$ and $M(KK)$ invariant mass spectra. The lines refer to the amplitudes given in the legend. (a) $M(KK)$ invariant mass spectrum and (b) $M(\gamma K)$ invariant mass spectrum.

explicitly distinguishing between resonant signals and non-resonant background contributions. The model was applied to the radiative decay $J/\psi \to \gamma ab$, incorporating rescattering effects between the final-state mesons. This framework includes the tree-level decay of J/ψ into the final-state pseudoscalar mesons, the cascade decay of J/ψ radiating into a resonance particle that subsequently decays into ab, the rescattering process where J/ψ radiates into ab, followed by final-state interactions, and the chain of J/ψ decaying into one pseudoscalar meson and an intermediate resonance, which then radiates another pseudoscalar meson via scattering. Additionally, the decay of the f_0 resonance includes contributions from meson rescattering. In contrast, conventional isobar models typically describe cascade decays through a BW parametrization of intermediate resonances, supplemented with ad hoc background terms. Such approaches often introduce arbitrariness in modeling background structures, leading to uncertainties in resonance parameter extraction. Our coupled-channel formalism, however, is constrained by ab scattering, providing a self-consistent description of both resonant and non-resonant effects, thereby minimizing model-dependent ambiguities. Despite its computational complexity, this approach offers significant theoretical advantages for practical data analysis.

For the three-body system γab, considering only ab coupled-channel effects is insufficient. Although photon-induced electromagnetic interactions are weak (allowing photon-meson rescattering to be neglected), an additional coupled-channel effect arises: the rescattering between a meson $\bar{X}$ (coupled the γa system) and another pseudoscalar meson. We derive the corresponding formalism to incorporate this process. Combining these four mechanisms, we establish a comprehensive theoretical framework for $J/\psi \to \gamma ab$, essential for future experimental analyses of this decay.

To illustrate the framework, we constructed a toy model for $J/\psi \to \gamma K_S K_S$, introducing two f_0-resonances and one K_1 meson. The f_0-resonances coupled to $K\bar{K}$, with additional contributions from the $\pi\pi$ coupled channel, form a two-bare-state, two-channel system. The K_1 meson couples to γK_S, as described earlier. By evaluating all four mechanisms, we compute the Dalitz plot and invariant mass spectra for $K_S K_S$ and γK_S. The results demonstrate that the peaks of the f_0-resonances emerge atop smooth backgrounds, while the K_1 peak exhibits significant distortion due to interference effects, deviating markedly from its nominal resonance profile. These findings highlight the necessity of a unified treatment of signals and backgrounds for correct experimental interpretation.

This study aimed to provide a coupled-channel-based amplitude analysis framework for the analysis of the extremely high-precision data and to advance the study of glueballs by taking coupled-channel effects into account in a self-consistent manner.

References

[1] P. A. Zyla *et al*. (Particle Data Group), Prog. Theor. Exp. Phys. **2020**, 083C01 (2020)
[2] A. Esposito, A. Pilloni, and A. Polosa, Phys. Rep. **668**, 1 (2017)
[3] M. Albaladejo, M. Battaglieri, L. Bibrzycki *et al*., *Snowmass white paper: Need for amplitude analysis in the discovery of new hadrons*, (2022), arXiv: 2203.08208 [hep-ph]
[4] S. X. Nakamura, Q. Huang, J. J. Wu *et al*., Phys. Rev. D **107**, L091505 (2023) [Erratum: Phys. Rev. D **109**, 039901 (2024)], arXiv: 2212.07904 [hep-ph]
[5] I. Aitchison, Nucl. Phys. A **189**, 417 (1972)
[6] H. Kamano, S. X. Nakamura, T. S. H. Lee *et al*., Phys. Rev. C **94**, 015201 (2016), arXiv: 1605.00363[nucl-th]
[7] I. Denisenko, A. V. Anisovich, V. Crede *et al*., Phys. Lett. B **755**, 97 (2016), arXiv: 1601.06092[nucl-ex]
[8] Y. F. Wang, EPJ Web Conf **291**, 02004 (2024), arXiv: 2401.01186[nucl-th]
[9] M. Ablikim *et al*., Phys. Rev. D **92**, 052003 (2015)
[10] M. Ablikim *et al*., Phys. Rev. D **98**, 072003 (2018)
[11] A. Rodas *et al*. (JPAC Collaboration), *Scalar and tensor resonances in j/ψ radiative decays*, (2021), arXiv: 2110.00027 [hep-ph]
[12] A. V. Sarantsev and E. Klempt, Int. J. Mod. Phys. A **39**, 2450096 (2024)
[13] A. Matsuyama, T. Sato, and T. S. H. Lee, Phys. Rept. **439**, 193 (2007), arXiv: nucl-th/0608051
[14] S. X. Nakamura, Q. Huang, J. J. Wu *et al*., Phys. Rev. D **109**, 014021 (2024), arXiv: 2311.05391[hep-ph]
[15] S. X. Nakamura and J. J. Wu, *Pole determination of $p_{\psi s}^{\lambda}(4338)$ and possible $p_{\psi s}^{\lambda}(4255)$ in $b^- \to J/\psi\lambda\bar{p}$*(2023), arXiv: 2208.11995 [hep-ph]
[16] C. D. Abell, D. B. Leinweber, Z. W. Liu *et al*., Phys. Rev. D **108**, 094519 (2023), arXiv: 2306.00337[hep-lat]
[17] S. He, X. Feng, and C. Liu, JHEP **2005**, 011 (2005)
[18] B. S. Zou and D. V. Bugg, *Covariant tensor formalism for partial wave analyses of psi decay to mesons*, (2002), arXiv: 0211457[hep-ph]
[19] J. J. Wu, T. S. H. Lee *et al*., Phys. Rev. C **85**, 044002 (2012), arXiv: 1202.1036[nucl-th]
[20] S. Willenbrock, *Mass and width of an unstable particle*, (2024), arXiv: 2203.11056[hep-ph]